IVYSPRING INTERNATIONAL PUBLISHER

Theranostics

2015; 5(2): 124-133. doi: 10.7150/thno.10014

Research Paper

$\alpha_v\beta_3$-targeted Copper Nanoparticles Incorporating an Sn 2 Lipase-Labile Fumagillin Prodrug for Photoacoustic Neovascular Imaging and Treatment

Ruiying Zhang[1*], Dipanjan Pan[2,3*], Xin Cai[1], Xiaoxia Yang[2], Angana Senpan[2], John S. Allen[2], Gregory M. Lanza[1, 2✉], and Lihong V. Wang[1✉]

1. Department of Biomedical Engineering, Washington University, St Louis, MO 63130;
2. Department of Medicine, Washington University School of Medicine, St Louis, MO 63108;
3. Current address: Department of Bioengineering and Beckman Institute, University of Illinois, Urbana, IL 61801.

*Authors: equal contribution.

✉ Corresponding authors: Lihong V. Wang, PhD. Department of Biomedical Engineering, Washington University, Whitaker Hall, Room 190D, Campus Box 1097, 1 Brookings Drive, St. Louis, MO 63130. Tel: (314) 935-6152. lhwang@wustl.edu And Gregory M. Lanza, MD PhD. Professor of Medicine and Bioengineering, Division of Cardiology, Washington University Medical School, CORTEX building, Suite 101, 4320 Forest Park Ave. Saint Louis, MO. Tel: (314) 454-8813 Greg.lanza@mac.com.

Received: 2014.06.30; Accepted: 2014.09.18; Published: 2015.01.01

Abstract

Photoacoustic (PA) tomography enables multiscale, multicontrast and high-resolution imaging of biological structures. In particular, contrast-enhanced PA imaging offers high-sensitivity noninvasive imaging of neovessel sprout formation and nascent tubules, which are important biomarkers of malignant tumors and progressive atherosclerotic disease. While gold nanoparticles or nanorods have been used as PA contrast agents, we utilized high-density copper oleate small molecules encapsulated within a phospholipid surfactant (CuNPs) to generate a soft nanoparticle with PA contrast comparable to that from gold. Within the NIR window, the copper nanoparticles provided a 4-fold higher signal than that of blood. $\alpha_v\beta_3$-integrin targeting of CuNPs in a Matrigel™ angiogenesis mouse model demonstrated prominent ($p<0.05$) PA contrast enhancement of the neovasculature compared with mice given nontargeted or competitively inhibited CuNPs. Furthermore, incorporation of a Sn 2 lipase-labile fumagillin prodrug into the CuNP outer lipid membrane produced marked antiangiogenesis in the same model when targeted to the $\alpha_v\beta_3$-integrin, providing proof of concept *in vivo* for the first targeted PA – drug delivery agent.

Key words: copper, nanoparticle, near-infrared imaging, photoacoustic imaging, angiogenesis imaging, anti-angiogenic therapy.

Introduction

As an important component of an expanding vascular network the neovasculature can be viewed as a biomarker of inflammation associated with tumor aggressiveness or atherosclerotic plaque progression. [1-3] To date, noninvasive imaging of angiogenesis has been essentially a preclinical endeavor, although imaging candidates have reached the clinical testing level for MRI and nuclear medicine. Nuclear medicine probes, although exquisitely specific for neovascular biosignatures, such as the $\alpha_v\beta_3$-integrin, are not specific to angiogenesis, since this adhesion molecule is activated on numerous cell types present in tumors or atherosclerotic lesions. [4-6] By comparison, MRI paramagnetic nanoparticle agents are often vascular-constrained by size and very specific for neoendothelial expression of $\alpha_v\beta_3$-integrin, but such agents

have experienced other roadblocks in the clinic. [7] Photoacoustic molecular imaging offers noninvasive vascular-constrained detection of angiogenic biomarkers with very high resolution imaging of the neovasculature.

Different imaging modalities have different characteristic resolution limits, with microscopic images having the highest resolution for thin specimens. For biomedical instrumentation, ultra-high spatial resolution MRI at 3.0T and high resolution CT provide *in vivo* blood vessel images but with a poorer resolution, in the range of 200 to 500 μm, which is inadequate for discrete neovessel imaging. [8-12] Photoacoustic (PA) imaging combines the advantages of ultrasound imaging and optical imaging and offers high depth-to-resolution ratios at different spatial scales, ranging from organelles to organs, [13] as well as unique and important physiological assessments, such as differential circulating blood oxygenation levels.

Previous studies have confirmed that PA imaging's utility can be markedly extended with exogenous contrast agents. [14-16] In many instances, these contrast agents have been based on gold cubes, spheres, or rods with particle sizes greater than the renal clearance threshold (<8 to 10 nm), creating difficult translational challenges when proving long-term safety in man. Gold nanobeacons (120-160 nm) were developed to achieve the large absorption cross-sections of bigger solid gold particles by suspending a multitude of small gold nanoparticles (3-5 nm) in a hydrophobic matrix encapsulated with phospholipid (160 nm). [17] Moreover, the optical absorption wavelength of nanoparticles was tunable well into the NIR optical window, minimizing endogenous absorption and maximizing PA imaging depth.

However, the pressure of healthcare economics has placed an emphasis on driving the costs of imaging studies down, and we have thus sought lower cost biocompatible alternatives to gold. We hypothesized that nanoparticles entrapping high densities of organically soluble small molecular weight copper complexes could provide an inexpensive and effective approach to neovascular targeted PA imaging. The choice of copper as a cheaper, biocompatible alternative to gold was independently supported by a recent report describing nontargeted crystalline copper sulfide nanoparticles as PA contrast agents for deep tissue imaging at 1064 nm. [18] In this research, a soft noncrystalline $\alpha_v\beta_3$-targeted copper-oleate nanoparticle ($\alpha_v\beta_3$-CuNP) was developed and its PA imaging signal with respect to blood and the previously reported gold nanobeacons was characterized [17] as a function of NIR wavelength and with varying nanoparticle concentrations. The *in vivo* efficacy of $\alpha_v\beta_3$-CuNPs for high-resolution imaging of mouse neovasculature was examined in a Matrigel™ model of angiogenesis. Furthermore, the theranostic antiangiogenic potential of $\alpha_v\beta_3$-CuNPs incorporating a novel Sn 2 lipase-labile fumagillin prodrug (Fum-PD) was also studied. [19]

Materials and Methods

Reagents

Unless otherwise listed, all solvents and reagents were purchased from Aldrich Chemical Co. (St. Louis, MO) and used as received. Anhydrous chloroform and methanol were purchased from Aldrich Chemical Co. Poly (styrene-*b*-acrylic acid) (PS-*b*-PAA) was purchased from Polymer Source Inc. (Montreal, Canada). High purity egg yolk phosphatidylcholine was purchased from Avanti Polar Lipids, Inc. Cholesterol and cooper oleate were purchased and used as received from Aldrich Chemical Co. (St. Louis, MO). Sorbitan monolaurate was purchased from Aldrich. Argon and nitrogen (Ultra High Purity: UHP, 99.99%) were used for storage of materials. The Spectra/Por membrane (Cellulose MWCO: 20,000 Da) used for dialysis was obtained from Spectrum Medical Industries, Inc. (Laguna Hills, CA).

Preparation of Sn 2 lipase labile Fumagillin prodrug

Synthesis of the Sn 2 prodrug was accomplished in two steps: 1) saponifying fumagillin dicyclohexylamine salt to fumagillol, and 2) esterifying the product with 1-palmitoyl-2-azelaoyl-sn-glycero-3-phosphocholine (PAzPC). [19] Briefly, fumagillin dicyclohexylamine salt (NCI) in 1:1 methanol:water was treated with 35% NaOH, stirred in an ice bath for 2 h, warmed to room temperature, treated with another equivalent of 35% NaOH, and then stirred in an ice bath until the starting material was not detected by TLC (~4 h). After evaporating the methanol and solubilizing in ethyl acetate, the mixture was extracted with 5% citric acid, brine, bicarbonate, and brine again, then dried with $MgSO_4$ and concentrated *in vacuo*. The crude product was purified with activated charcoal in acetonitrile and then filtered through a celite pad. (Yield: a colorless solid, 59 mg (70%). 1H NMR (CD_3OD): δ 5.20 (t, 1H), 4.3 (m, 1H), 3.42 (m, 1H), 3.38 (s, 3H), 2.88 (d, 1H), 2.63 (t, 1H), 2.51 (d, 1H), 2.1–2.3 (m, 2H), 2.2 (m, 1H), 1.89 (d, 1H), 1.7–1.9 (m, 2H), 1.8 (d, 3H), 1.7 (d, 3H), 1.17 (s, 3H), 0.96 (m, 1H). HR-MS found: MH+ (283.3).

A solution of C16-09:0 (COOH) PC 1-hexadecyl-2-azelaoyl-sn-glycero-3-phosphocholine, followed by 4-dimethylaminopyridine (DMAP) and

N, N'-dicyclohexyl-carbodiimide (DCC), was added to fumagillol in dry dichloromethane. The reaction mixture was stirred overnight at ambient temperature then passed over a short pad of silica gel using EtOAc/n-hexane. The filtered solvent was removed *in vacuo*, and the oil residue was purified by column chromatography on SiO_2 using EtOAc/n-hexane for elution to yield the fumagillin prodrug (Fum-PD) compound as a pale yellowish solid (yield: 54%). 1H NMR ($CDCl_3$): δ 0.88 (t, 3H), 1.22–1.37 (m, 37H), 1.58–1.96 (m, 20H), 2.26–2.60 (m, 7H), 3.40 (m, 12H), 3.48 (m, 3H), 3.86–4.00 (m, 4H), 4.10–4.37 (m, 5H), 5.21 (m, 1H). HR-MS found: 930.6 (MH+).

Preparation of copper nanoparticles

Copper-oleate (260 mg) dissolved in toluene was suspended in almond oil (4 ml), gently vortexed to homogeneity, and filtered through a small bed of cotton. The solvent was evaporated under reduced pressure at 45°C, leaving a mixture containing 65 mg of copper oleate per ml. The surfactant co-mixture included high-purity egg yolk phosphatidylcholine (91.9 mol%), cholesterol (8 mol%), and $\alpha_v\beta_3$-peptidomimetic antagonist conjugated to PEG_{2000}-phosphatidylethanolamine (0.1 mol%; Kereos, St. Louis, MO, USA). Therapeutic $\alpha_v\beta_3$-CuNPs incorporated the Sn 2 lipase labile fumagillin prodrug (2.28 mol%) at the equimolar expense of phosphatidylcholine. The surfactant co-mixtures were dissolved in chloroform, evaporated under reduced pressure, dried in a 40°C vacuum oven overnight, and dispersed into water by probe sonication. This suspension was combined with the copper oleate-almond oil mixture (20% v/v), distilled deionized water (77.3% w/v), and glycerin (1.7%, w/v) and continuously processed at 20,000 psi for 4 min with an S110 Microfluidics emulsifier (Microfluidics, Newton, MA, USA) at 4°C. The copper nanoparticles (CuNPs) were dialyzed against water using a 20-kDa MWCO cellulose membrane for a prolonged period of time and then passed through a 0.45 µm Acrodisc syringe filter (Pall Life Sciences, East Hills, NY, USA). To inhibit lipid oxidation, the CuNPs were stored under an argon atmosphere, typically at 4°C. (**Figure 1**)

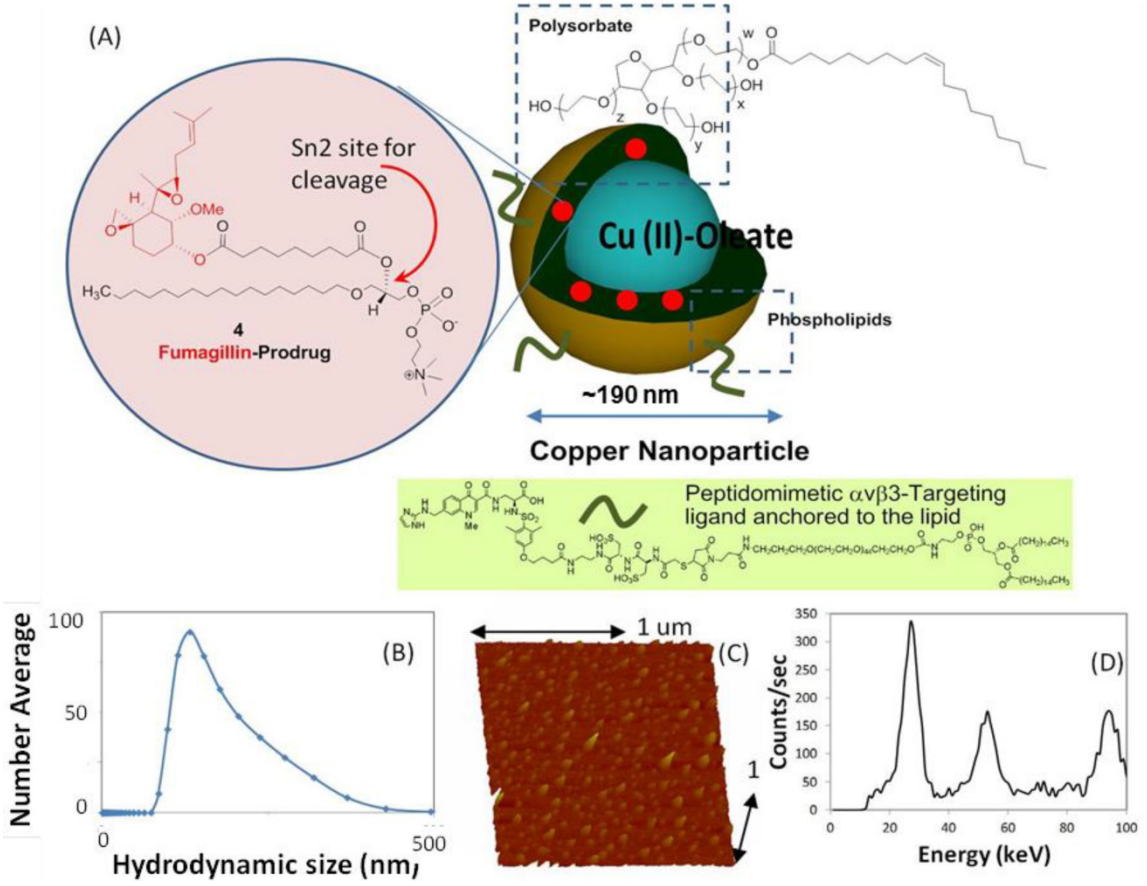

Figure 1. Synthesis and physiochemical characterization of CuNPs. (a) schematic of the concept of CuNPs with fumagillin prodrug; (b) hydrodynamic particle size distribution from DLS. The nominal hydrodynamic diameters of $\alpha_v\beta_3$-CuNPs and fumagillin prodrug CuNPs were typically 190 nm ± 15 nm, (c). Anhydrous state atomic force microscopy (AFM) image of CuNPs (drop-deposited on glass) Average height: 80 nm ± 12 nm. (d). EDX spectrum generated from the SEM image.

The nominal hydrodynamic diameter (D_h) of the $\alpha_v\beta_3$-CuNPs and the fumagillin prodrug CuNPs was determined by dynamic light scattering (DLS) measurements (Brookhaven ZetaPlus, Brookhaven Instruments Corporation) in aqueous solution, were typically 190 nm ± 15 nm (std error), with a polydispersity of 0.09 ± 0.01, and a zeta potential of -23 ± 06 mV. Incorporation of the prodrug at 2.28 mol% (~0.5 mM) within the surfactant co-mixture had negligible impact on particle sizes.

The $\alpha_v\beta_3$-integrin antagonist was a quinalone nonpeptide developed by Lantheus Medical Imaging (Billerica, MA, USA) and synthesized by Kereos (U.S. Patent 6,511,648 and related patents). The vitronectin antagonist was reported and characterized as the ^{111}In-DOTA conjugate RP478 and cyan 5.5 homologue TA145. [20] The homing specificity of the ligand was demonstrated and characterized with Matrigel plug implanted in *Rag1*^{tm1Mom} Tg (Tie-2-lacZ) 182-Sato and C57Bl/6 mice. [14]

The reference gold nanobeacons (GNBs) used in this study were prepared and characterized as previously described. [14] The GNBs were in a 20 vol% suspension with a nominal particle size of 160 nm, containing 6120 gold-oleate particles (3-5 nm)/nanobeacon, with a gold content of 1080 μg/g.

Matrigel™ plug mouse model of angiogenesis

All animal studies were conducted in accordance with protocols approved by the Animal Care and Use Committee of Washington University Medical School.

Athymic nude-mice (Harlan Labs, Indianapolis, IN) with body weights ranging from 23 to 27 g were obtained. Anesthesia was induceod by ketamine (100 mg/ml) and xylazine (20 mg/ml), which were maintained with 0.5% to 1% isoflurane in oxygen, with ventilator support and supplemental temperature support. Matrigel (0.5 ml, BI, Biosciences, San Jose, CA, USA) enriched with fibroblast growth factor-2 (500 nm/ml; Sigma-Aldrich, St. Louis, MO, USA) and heparin was implanted subcutaneously along the mouse flank. The nude mice (n = 12) were randomly distributed into four groups to test (1) the efficacy of $\alpha_v\beta_3$-CuNPs for PA molecular imaging of angiogenesis *in vivo* and (2) the efficacy of $\alpha_v\beta_3$-CuNPs with Fum-PD as a theranostic agent. For the first test, three groups were compared on day 18 using PA imaging: (1) $\alpha_v\beta_3$-CuNPs without Fum-PD (integrin targeted, n=3); (2) nontargeted CuNPs (nonspecific entrapment, n=3) and (3) $\alpha_v\beta_3$-almond oil nanoparticle (NP) followed after 10 min by $\alpha_v\beta_3$-CuNPs without Fum-PD (specific competition, n=3). To address the second question within the same experimental design, (4) $\alpha_v\beta_3$-CuNPs with Fum-PD were administered on days 11 and 15, following Matrigel implantation, and the effect on angiogenesis was assessed on day 18 with $\alpha_v\beta_3$-CuNPs without Fum-PD (n=3). All treatments were injected via tail vein at 2 μl/g body weight of the 20 vol% nanoparticle suspensions. For each animal dynamic PA imaging was performed before injection (baseline, 0 min) and then repeated every 30 min over 270 minutes post-injection.

Photoacoustic imaging

A reflection-mode PA imaging system using dark-field ring-shaped illumination [21] was pumped by a Q-switched Nd:YAG (LS-2137; Lotis TII) laser with <15-ns pulse duration and a 10-Hz pulse repetition rate. The light energy on the sample surface was controlled to conform to the American National Standards Institute (ANSI) standard for maximum permissible exposure. A 10 MHz central frequency, spherically focused (2.54 cm focus length, 1.91 cm diameter active area element, and 68% nominal bandwidth (One way -6 dB bandwidth is ~96%) ultrasonic transducer (V315; Panametrics-NDT, Waltham, MA, USA) acquired the generated PA signals. The signal was amplified by a low-noise amplifier (5072PR; Panametrics-NDT), and recorded using a digital oscilloscope (TDS 5054; Tektronix, Beaverton, OR, USA) with 50-MHz sampling. PA signal fluctuations due to pulse-to-pulse energy variation were compensated for by signals from a photodiode (DET110; Thorlabs, Newton, NJ, USA), which sampled the energy of each laser pulse.

Prior to *in vivo* imaging, two preliminary experiments were performed. In preliminary experiment 1, individual samples of CuNPs (20 vol%) and bovine blood (hct. ~45%) were placed into individual transparent plastic tubes (ID, 510 μm) and imaged by the PA system at 767 nm. The A-line signals from these two tubes are presented in **Figure 2** as superimposed waveforms.

In preliminary experiment 2, the transparent Tygon tubes (ID, 510 μm) were filled with CuNPs (20 vol %), GNBs (20 vol%), and whole bovine blood (hct. ~45%). They were imaged at varying wavelengths between 730 nm and 830 nm. As an extension of this experiment, CuNPs were serially diluted from 6.0 μM to 0.17 μM and imaged at 750 nm, 760 nm, 770 nm, 780 nm, and 790 nm. In each experiment, the maximum amplitudes of the A-line signals (n=5) at each wavelength were averaged.

Finally, *in vivo* imaging of angiogenesis in the Matrigel Plug model was performed. A linear translation stage (XY-6060; Danaher Motion, Rad ford, VA, USA) was used for raster scanning to obtain 3-D PA data. A computer controlled the stage and synchronized it to the data acquisition. To shorten the data acquisition time, a continuous scan was used without

signal averaging. Typical scanning values are as follows: voxel dimensions, 0.1 × 0.2 mm; laser pulse repetition rate, 10 Hz; acquisition time, ~20 min.

In vivo imaging was performed using ventilated anesthetized mice with shaved flanks, constantly warmed to 37°C by a heating block and positioned immediately beneath the transparent clear membrane. PA imaging was performed at 767 nm, as previously used for GNB *in vivo.* [14] Similarly, the vessel-integrated PA amplitude, calculated by integrating the enveloped PA signal amplitude over the blood vessel region, was used to quantify the degree of angiogenesis. The vessel-integrated PA amplitude was normalized to that of the pretreatment level during the analysis.

Statistical Analysis

Data were analyzed using analysis of variance (GraphPad Prism Ver. 6.03) ($p < 0.05$). Data are presented as the mean ± standard error of the mean unless otherwise stated.

Results

Given the inherently strong PA signal of hemoglobin, the efficacy of PA contrast agents for targeted molecular imaging of neovascular integrin expression is dependent on the strength and differentiation of its signal from the blood background. The PA signal of CuNPs (20 vol%) was compared with whole bovine blood (45% hct.) at 767 nm. As seen in **Figure 2**, the time-aligned PA signal of the copper NP emulsion was markedly greater than that of the bovine blood at 767. The peak-to-peak signal of the CuNPs (2.3 a.u.) was 4-fold greater than that of blood (0.58 a.u.) at 767 nm, suggesting that the PA signal of neovascular bound CuNPs could be readily detectable *in vivo*.

GNBs have been previously shown to produce strong PA contrast *in vivo* when applied to sentinel lymph node imaging or when targeted to neovasculature *in vivo.* [14, 17, 22, 23] The PA signal enhancement of CuNPs relative to blood (45% hct.) was compared to the signal of GNBs relative to blood across a NIR frequency range of 730 nm to 830 nm (**Figure 3**) on an equal nanoparticle number basis. Over almost the entire spectrum, the CuNPs signal strength relative to blood was around 5-fold greater with a noticeable decline beyond 820 nm. In general, the PA ratios of GNBs and CuNPs were very similar except between 760 nm and 790 nm, with the greatest divergence between GNBs and CuNPs at 770 nm, at which point the gold contrast result was nearly twice that of copper. GNB particles experienced the same declining results as CuNPs from 800 nm and beyond.

The concentration dependence of CuNPs' signals as a function of frequency was examined. CuNPs were serially titrated from 6.0 μM to 0.17 μM and studied at NIR wavelengths between 750 nm and 790 nm (**Figure 4 (A)**). PA amplitude decreased with reductions in CuNP concentration level, but the magnitude of signal diminishment was generally less than the percent change in CuNP level. This was particularly notable for the higher concentrations, between 6.0 μM and 1.5 μM. The magnitude of the CuNP's PA signal was greatest at 750 nm and 760 nm. At higher wavelengths, the magnitude of the CuNP signal trended lower, with the greatest contrast loss seen at the lower CuNP concentrations. It can be calculated from the extinction coefficient spectrum shown in **Figure 4 (B)** that the extinction coefficient of CuNPs at 700 nm was 1.3 times as strong as that at around 770 nm. However, the laser energy at 767 nm (the peak of laser energy) is an order of magnitude stronger than that at 700 nm. Therefore, neovascular imaging signal peaks around 767 nm.

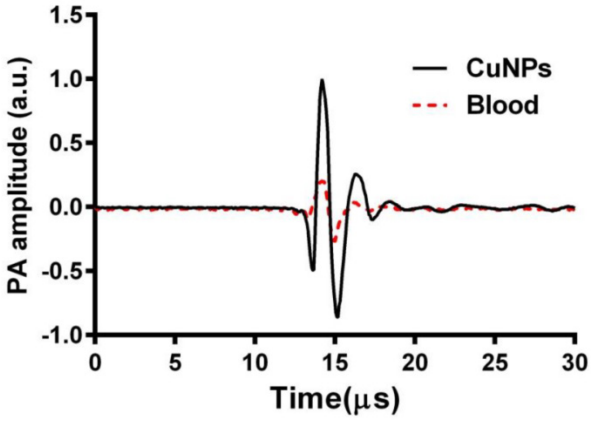

Figure 2. Overlay of PA signals from CuNPs (20 vol%) and blood (whole bovine blood, hct. 45%;). CuNPs and blood samples were placed into transparent Tygon™ tubes (ID = 510 μm) and imaged by the PA system at 767 nm. The peak-to-peak PA signal from the CuNPs was 4 times greater than that of the blood at 767 nm.

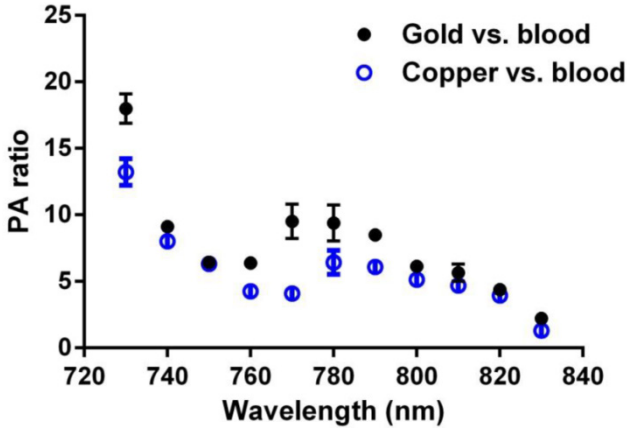

Figure 3. Equal-nanoparticle-based ratio of peak-to-peak PA signal amplitudes from previously reported gold nanobeacons (20 vol%) [14] and CuNPs (20 vol%) to those of whole bovine blood (hct. 45%) over the 730 – 830 nm range. Over the whole spectrum, PA signals of CuNPs were markedly greater than those of the blood. In general, the PA ratios of GNBs and CuNPs relative to blood were similar.

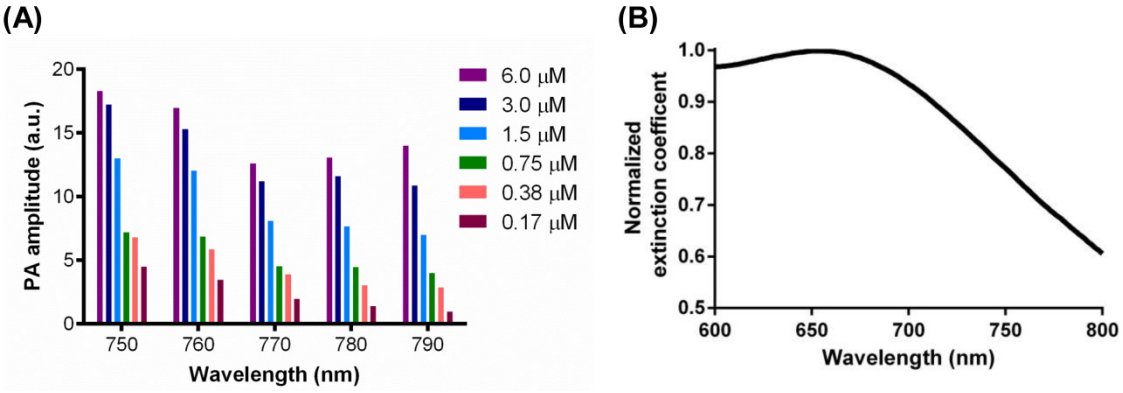

Figure 4. (A) PA signals from copper nanoparticles (20 vol%) in a transparent Tygon tube filled with serially diluted copper nanoparticles (0.17 μM, 0.38 μM, 0.75 μM, 1.5 μM, 3.0 μM, 6.0 μM) at laser wavelengths from 750 nm to 790 nm, with 10 nm step size. A nonlinear relationship between the PA amplitude and CuNP concentration was observed. (B) Normalized extinction coefficient spectrum of the CuNPs (20 vol%) at laser wavelengths from 600 nm to 800 nm.

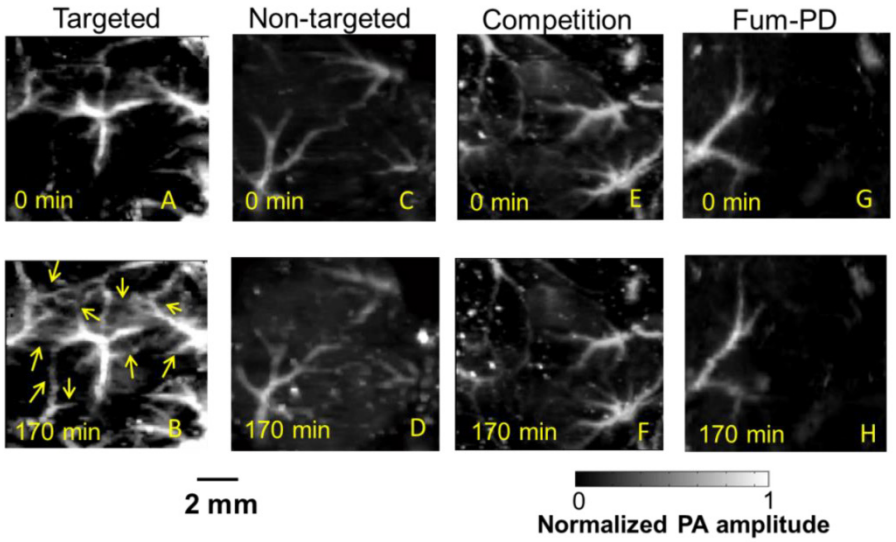

Figure 5. *In vivo* PA images of the Matrigel plug area implanted in 4 groups of mice 18 days prior to imaging. (A)-(B) Targeted CuNPs group: mice received $\alpha_v\beta_3$-CuNPs just before PA imaging. The enhanced neovasculature is marked by arrows in B. (C)-(D):Nontargeted CuNPs group: mice received nontargeted CuNPs right before PA imaging (E)-(F):Competition group: mice received a competitive dose of $\alpha_v\beta_3$-oil only NP (1:1) 10 minutes prior to imaging, followed by $\alpha_v\beta_3$-CuNPs right before imaging. (G)-(H) Fum-PD group: mice received $\alpha_v\beta_3$-CuNPs with Fum-PD 11 and 15 days after the Matrigel implantation, and $\alpha_v\beta_3$-CuNPs w/o Fum-PD right before PA imaging. Comparing the PA images of the nontargeted, competition, and Fum-PD groups at 0 min and 170 min, very little change in PA signals can be found. For all PA images, laser wavelength = 767 nm.

To provide robust assessment of PA signal enhancement due to the CuNPs, *in vivo* neovascular imaging was studied in the Matrigel plug model in mice. Mice implanted with Matrigel™ 18 days previously received either $\alpha_v\beta_3$-CuNPs, nontargeted CuNPs, or $\alpha_v\beta_3$-CuNP preceded by 10 minutes with a competitive dose $\alpha_v\beta_3$-oil only NPs (1:1). As seen in **Figure 5**, at 0 min, forming neovessels were observed by the inherent PA contrast imparted by erythrocyte hemoglobin. The magnitude of the signal varied among animals with the extent of neovascular proliferation. Following $\alpha_v\beta_3$-CuNP injection, the magnitude of the PA signal in these immature tubules clearly increased, and numerous incomplete vascular sprouts appeared, as we have previously reported for GNBs. [14] The formation of the neovessel shoots depicted an early evolution stage of a dense and irregular microvasculature. In contradistinction to the animals receiving $\alpha_v\beta_3$-CuNPs, those given nontargeted-CuNPs had very little increase in the vessel-integrated PA amplitude. As shown, a minimal passive accumulation of the CuNPs in the forming bridges and sprouts combined with a modest amount of blood pool enhancement relative to the neovessel tubules at 0 min. We have previously reported that blood pool enhancement for GNBs in the intact microvasculature surrounding the Matrigel implant was negligible, [14] but within the plug, the slow moving blood may be associated with very slow washout. In the competition group at 170 min, very little change in the PA signal from the forming vascular tubules or sprouts was observed. In this group, the pretreatment binding of the $\alpha_v\beta_3$-oil NPs appeared to have blocked most of the receptors for the $\alpha_v\beta_3$-CuNP and even precluded significant passive accumulation. **Figure 6** presents the average change in the vessel-integrated

PA amplitude between the three treatment groups, showing that the $\alpha_v\beta_3$-CuNPs increased PA contrast, while the nontargeted-CuNP did not (p<0.05). Moreover, the specificity of targeting the neovasculature was again demonstrated by the low vessel-integrated PA amplitude measured in the competition group versus the $\alpha_v\beta_3$-CuNP group (p<0.05), and even relative to the nontargeted control. Dynamic accumulation of PA contrast measured in the $\alpha_v\beta_3$-CuNP group increased progressively over the 230 minutes post injection interval (**Figure 7**).

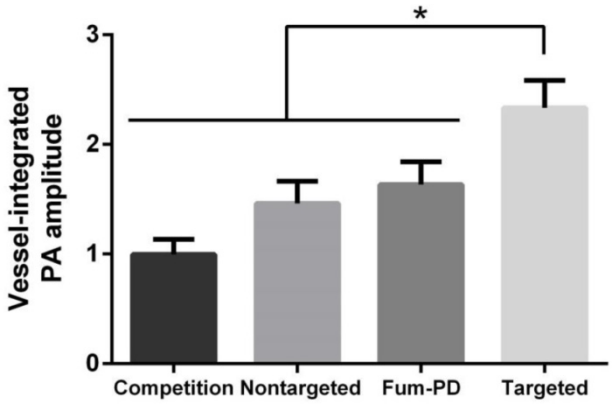

Figure 6. Vessel-integrated PA amplitude (normalized to the baseline, i.e., the vessel-integrated PA amplitude at 0 min) at 170 min post-injection for four groups of mice. The vessel-integrated PA amplitude for the $\alpha_v\beta_3$-targeted group increased more than that of the other three groups (*P<0.05). Almost no increase in vessel-integrated PA amplitude was measured in the competition group, and a slight increase was observed in the non-targeted and Fum-PD groups.

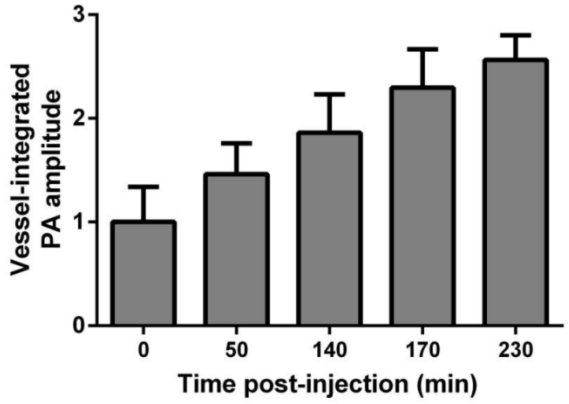

Figure 7. Vessel-integrated PA amplitude *vs.* post-injection time for the $\alpha_v\beta_3$-CuNPs group. The vessel-integrated PA amplitude increased progressively over the 230 min post injection interval.

In a second aspect of the Matrigel™ angiogenesis experiment, fumagillin-prodrug (Fum-PD), [24, 25], was incorporated into the phospholipid surfactant at 2.28 mol%. The chemical synthesis, characterization, and *in vivo* effectiveness of Fum-PD incorporated into perfluorocarbon nanoparticles has been previously reported. [19, 26] $\alpha_v\beta_3$-CuNP (2 µl/g) incorporating Fum-PD was administered on days 11 and 15 post Matrigel™ implant, and the vessel-integrated PA amplitude in these animals was determined on day 18. At baseline, the amount of neovasculature observed by PA imaging was sparse, but no more so than that in the other groups. Moreover, following $\alpha_v\beta_3$-CuNP injection there was little sprouting enhancement at 170 minutes. As shown collectively in **Figures 5 and 6**, the vessel-integrated PA amplitude change was similar to that measured in the nontargeted-CuNP group, and appeared related to modest particle accumulation in the nascent tubules, with less signal related to sprout formation. Although drug delivery and imaging were not performed simultaneously to minimize the differential animal handling between the groups, these results illustrated the potential of CuNPs as vehicles for drug delivery and diagnosis.

Discussion

Photoacoustic imaging has demonstrated broad applications in the imaging and physiological characterization of the vasculature, particularly the microvasculature [13, 27], and microvascular expansion driven by brain tumor hypoxia [28]. The vascular endothelium provides numerous "road-signs" reflecting its developmental stage, as seen for the neovasculature, or its state of activation, as seen with inflammation. In each instance, specific PA characterization depends on molecular imaging through the recognition of unique endothelial biomarkers. [15, 16, 22, 29-33] In the present study, sparse activated $\alpha_v\beta_3$-integrin was selected as a biomarker of angiogenesis. While we have previously reported dynamic imaging of the forming neovasculature with gold nanobeacons, the high and unpredictable cost of gold, and the unclear long-term safety of larger nonmetabolizable nanoparticles, such as carbon fullerenes or nanotubes, led to the design and development of CuNPs. While free copper can elicit systemic toxicity, CuNPs are comprised of high densities of small organometallic complexes that can be eliminated through the bile or urine, minimizing the risk potential for this agent. [34] In the present study, CuNPs offered comparable PA contrast enhancement, on an equal particle basis, to GNBs both *in vitro* and *in vivo*.

In vivo PA imaging was performed at 767 nm, which was optimal for the previously targeted GNB agent, but the spectral assessments of CuNP relative to blood and as a function of particle concentration suggest 740 or 750 nm may be preferred for targeting sparse epitopes like adhesion molecules. Also, the time for maximum neovascular signal was found to be nearly 4 hours in the Matrigel model, but similar particles administered *in vivo* for deeper-tissue angiogenesis imaging with MRI were shown to provide minimal targeting benefit after 2 hours. [35, 36] The difference likely relates to vascular vasoconstriction

with reduced blood flow to the skin in the subcutaneous Matrigel implant model, which is aggravated by the cooling effects of acoustically coupling the PA probe to the body during anesthesia, despite provision of supplemental heating to maintain core body temperatures. Lastly, CuNPs were designed to be vascular constrained agents to reduce nonspecific signal generated by interactions with extravascular cells expressing the $\alpha_v\beta_3$-integrin. Close examination of the 170-minute PA images in **Figure 5** showed negligible extravasation of the particles. Although much attention has been attributed to the leakiness of angiogenesis, even in the sprouting regions where the neovasculature is essentially open-ended, no evidence of nanoparticle accumulation beyond the tips of the forming neovessel branches was noted. Moreover, this was a consistent observation, regardless of whether the nanoparticles were integrin-targeted or not.

Fumagillin prodrug was incorporated into the phospholipid surfactant of CuNPs and demonstrated to elicit anti-angiogenic effects in this Matrigel model. Microanatomically, the treatment virtually eliminated the rich web of sprouts in the mice receiving $\alpha_v\beta_3$-CuNPs without Fum-PD. "Pruning" of neovasculature was first suggested by Jain in a visionary manner, but in this study, the concept was visually apparent. [37-39] Despite all of the extensive clinical research on the effects and benefits of anti-angiogenesis therapy in cancer and selected other pathologies, virtually all of the work has centered on vascular endothelial growth factor (VEGF) inhibition. While VEGF is a clear driver of angiogenesis, it elicits pleotropic effects and is not solely responsible for neovascularization. [40] Moreover, VEGF is produced by a variety of cell types, making effective blockade of the growth factor challenging. Typically, relatively high dosages of medicants are used clinically and these treatments have well known side-effects. [41]

As reported by others, fumagillin is an antiangiogenic agent which is specific for proliferating endothelial cells, but its clinical analogue, TNP-470, possessed only antidotal effectiveness in the clinic at the high doses required, which were accompanied by numerous toxicities, including neurocognitive dysfunction. [42-44] Fumagillin can be effectively incorporated into the phospholipid surfactant of nanoparticles for targeted delivery of anti-angiogenesis therapy through a mechanism referred to as "contact facilitated drug delivery" (CFDD) at a small fraction of the dosages previously used systemically. [2, 45, 46] Tethering of the lipid-encapsulated nanoparticle to the target cell surface facilitates the interaction and hemifusion of the two lipid membranes, which affords the passive transfer of the drug and phospholipids from the nanoparticle surface to the outer leaflet of the target cell membrane. The drug is then translocated to the inner leaflet through an ATP-dependent mechanism. [47, 48] CFDD eliminates the need for particle internalization with subsequent endosomal drug payload escape.

However, pharmacokinetic studies showed that fumagillin dissolved into the lipid membrane was substantially lost prematurely during circulation to the target neovasculature, despite its effectiveness *in vivo*. Fum-PD was developed to address this early release by coupling the drug through the Sn 2 acyl position (i.e., the stereospecific hydroxyl group of the second carbon of glycerol). Subsequent transfer of the monolayer components into the target cell membrane allows cytosolic phospholipases to enzymatically cleave the Sn 2 ester and release the drug, allowing it to diffuse into the cytosol for effect. Fum-PD as well as other similar prodrug compounds is incorporated stably into the hydrophobic aspects of the particle membrane. Importantly, Sn 2 lipase-labile prodrugs within the particle lipid membrane are stable in blood and plasma, even in the presence of excess exogenous lipase, and do not passively exchange to co-circulating RBC. [49] The results of the present research show the first example of a systemically targeted antiangiogenic drug delivery with a photoacoustic contrast nanoparticle. Given the rapid developments in hardware and software for PA imaging, one can envision numerous medical applications for low-cost CuNPs particles to target neovascular or alternative endothelial biosignatures for diagnostic and theranostic purposes.

Unlike current VEGF inhibitors, fumagillin-prodrug specifically targeted to angiogenic vessels suppresses angiogenesis, clinical disease, and inflammation in a preclinical model of rheumatoid arthritis (RA). [50] Enhanced endothelial nitric oxide (NO) modulates local macrophage inflammatory activity through NO activation of AMP-activated protein kinase (AMPK). *In vivo*, NO-induced AMPK activation increased autophagy by inhibiting mammalian target of rapamycin (mTOR) activity. Increased autophagy mediated the degradation of IkappaB kinase (IKK) and suppressed NF-κB. The suppression of NF-κB was associated with diminished inflammatory cytokine release. Importantly, the NO mediated inhibition of inflammation was reversed *in vitro* and *in vivo* by the co-administration of N(G)-nitro-L-arginine methyl ester (L-NAME), a nitric oxide synthase inhibitor. These unique anti-angiogenic and anti-inflammatory properties of Fum-PD nanotherapy may be applicable to the treatment of other angiogenesis-dependent diseases.

Conclusion

Soft copper oleate nanoparticles were synthesized and conceptually shown to offer effective photoacoustic contrast comparable to gold-based agents, but at a much lower cost and higher material availability. CuNPs possessed strong PA contrast relative to blood from 730 nm to 830 nm, which was similar to the PA signal response of gold nanobeacons relative to blood overall. In the Matrigel angiogenesis model, $\alpha_v\beta_3$-CuNPs markedly enhanced neovessel tubules and identified a myriad of incomplete emergent neovascular sprouts, which were not well detected or specifically differentiated as angiogenesis with inherent PA imaging. $\alpha_v\beta_3$-CuNPs effectively delivered fumagillin-prodrug, a potent anti-angiogenic therapy, *in vivo*, providing the first example of a systemically targeted drug delivery therapy with a photoacoustic contrast agent.

Abbreviations

PA: photoacoustic; CuNPs: copper oleate nanoparticles; Sn 2: glycerophospholipids use "sn" notation, stereospecific numbering. By convention the hydroxyl group of the second carbon of glycerol (Sn 2) is on the left on a Fischer projection; NIR: near infrared; $\alpha_v\beta_3$: alpha v beta 3 integrin; MRI: magnetic resonance imaging; CT: computed tomography; PET: positron emission tomography; $\alpha_v\beta_3$-CuNP: αvβ3-targeted copper oleate nanoparticle; Fum-PD: fumagillin prodrug; PS-*b*-PAA: poly(styrene-*b*-acrylic acid); DOTA: 1,4,7,10-tetraazacyclododecane-1,4,7,10-tetraacetic acid; Tie-2: endothelium-specific receptor tyrosine kinase; GNB: gold nanobeacons; PAzPC: 1-palmitoyl-2-azelaoyl-sn-glycero-3-phosphocholine; DMAP: dimethylaminopyridine; DCC: dicyclohexylcarbodiimide; DLS: dynamic light scattering; NP: nanoparticle; ID: inner diameter; hct: hematocrit; VEGF: vascular endothelial growth factor; CFDD: contact facilitated drug delivery. RA, rheumatoid arthritis. NO, nitric oxide. AMPK, AMP-activated protein kinase. mTOR, mammalian target of rapamycin. IKK, IkappaB kinase. L-NAME, L-arginine methyl ester.

Acknowledgement

The authors would like to thank Prof. James Ballard for his close reading of the manuscript. L. V. Wang has a financial interest in Microphotacoustic, Inc. and Endra, Inc., which did not support this work. Washington University owns the intellectual property to CuNP and it was licensed nonexclusively to Ocean NanoTech, LLC for research commerce. Kereos, Inc. provided the peptidomimetic homing ligand as a gift, and GML is a scientific co-founder of Kereos. The financial support from the NIH and DOD under grant numbers DP1 EB016986 (NIH Director's Pioneer Award), R01 CA186567 (NIH Director's Transformative Research Award), R01 EB016963, R01 CA159959, HL112518, HL113392, CA154737, CA136398, NS073457, and from the DOD CA100623 was greatly appreciated.

Competing Interests

The authors have declared that no competing interest exists.

References

1. Brooks PC, Clark R, Cheresh DA. Requirement of vascular integrin alpha v beta 3 for angiogenesis. Science. 1994; 264: 569-71.
2. Winter PM, Neubauer AM, Caruthers SD, Harris TD, Robertson JD, Williams TA, et al. Endothelial αvβ3 integrin–targeted fumagillin nanoparticles inhibit angiogenesis in atherosclerosis. Arterioscler Thromb Vasc Biol. 2006; 26: 2103-9.
3. Winter PM, Schmieder AH, Caruthers SD, Keene JL, Zhang H, Wickline SA, et al. Minute dosages of αvβ3-targeted fumagillin nanoparticles impair Vx-2 tumor angiogenesis and development in rabbits. FASEB J. 2008; 22: 2758-67.
4. Schnell O, Krebs B, Carlsen J, Miederer I, Goetz C, Goldbrunner RH, et al. Imaging of integrin αvβ3 expression in patients with malignant glioma by [18F] Galacto-RGD positron emission tomography. Neuro Oncol. 2009; 11: 861-70.
5. Beer AJ, Haubner R, Goebel M, Luderschmidt S, Spilker ME, Wester HJ, et al. Biodistribution and pharmacokinetics of the alphavbeta3-selective tracer 18F-galacto-RGD in cancer patients. J Nucl Med. 2005; 46: 1333-41.
6. Kenny LM, Coombes RC, Oulie I, Contractor KB, Miller M, Spinks TJ, et al. Phase I trial of the positron-emitting Arg-Gly-Asp (RGD) peptide radioligand 18F-AH111585 in breast cancer patients. J Nucl Med. 2008; 49: 879-86.
7. Pham CT, Mitchell LM, Huang JL, Lubniewski CM, Schall OF, Killgore JK, et al. Variable antibody-dependent activation of complement by functionalized phospholipid nanoparticle surfaces. J Biol Chem. 2011; 286: 123-30.
8. Costouros NG, Diehn FE, Libutti SK. Molecular imaging of tumor angiogenesis. J Cell Biochem. 2002; 87: 72-8.
9. Neeman M. Functional and molecular MR imaging of angiogenesis: seeing the target, seeing it work. J Cell Biochem Suppl. 2002; 39: 11-7.
10. Pearlman JD, Laham RJ, Post M, Leiner T, Simons M. Medical imaging techniques in the evaluation of strategies for therapeutic angiogenesis. Curr Pharm Des. 2002; 8: 1467-96.
11. Weissleder R. Scaling down imaging: molecular mapping of cancer in mice. Nat Rev Cancer. 2002; 2: 11-8.
12. Weissleder R, Ntziachristos V. Shedding light onto live molecular targets. Nat Med. 2003; 9: 123-8.
13. Wang LV, Hu S. Photoacoustic tomography: in vivo imaging from organelles to organs. Science. 2012; 335: 1458-62.
14. Pan D, Pramanik M, Senpan A, Allen JS, Zhang H, Wickline SA, et al. Molecular photoacoustic imaging of angiogenesis with integrin-targeted gold nanobeacons. FASEB J. 2011; 25: 875-82.
15. De La Zerda A, Zavaleta C, Keren S, Vaithilingam S, Bodapati S, Liu Z, et al. Carbon nanotubes as photoacoustic molecular imaging agents in living mice. Nat Nanotechnol. 2008; 3: 557-62.
16. Xiang L, Yuan Y, Xing D, Ou Z, Yang S, Zhou F. Photoacoustic molecular imaging with antibody-functionalized single-walled carbon nanotubes for early diagnosis of tumor. J Biomed Opt. 2009; 14: 021008-7.
17. Pan D, Pramanik M, Senpan A, Yang X, Song KH, Scott MJ, et al. Molecular photoacoustic tomography with colloidal nanobeacons. Angew Chem Int Ed. 2009; 48: 4170-3.
18. Li Y, Lu W, Huang Q, Huang M, Li C, Chen W. Copper sulfide nanoparticles for photothermal ablation of tumor cells. Nanomedicine (Lond). 2010; 5: 1161-71.
19. Pan D, Sanyal N, Schmieder AH, Senpan A, Kim B, Yang X, et al. Antiangiogenic nanotherapy with lipase-labile Sn-2 fumagillin prodrug. Nanomedicine. 2012; 7: 1507-19.
20. Meoli DF, Sadeghi MM, Krassilnikova S, Bourke BN, Giordano FJ, Dione DP, et al. Noninvasive imaging of myocardial angiogenesis following experimental myocardial infarction. J Clin Invest. 2004; 113: 1684-91.
21. Song KH, Wang LV. Deep reflection-mode photoacoustic imaging of biological tissue. J Biomed Opt. 2007; 12: 060503.
22. Pan D, Pramanik M, Wickline SA, Wang LV, Lanza GM. Recent advances in colloidal gold nanobeacons for molecular photoacoustic imaging. Contrast Media Mol Imaging. 2011; 6: 378-88.
23. Pan D, Pramanik M, Senpan A, Ghosh S, Wickline SA, Wang LV, et al. Near infrared photoacoustic detection of sentinel lymph nodes with gold nanobeacons. Biomaterials. 2010; 31: 4088-93.

24. Sudoi K, Kanamarui T, Brem H, Foikman J. Synthetic analogues of fumagillin that inhibit angiogenesis and suppress tumour growth. Nature. 1990; 348: 6.
25. Liu S, Widom J, Kemp CW, Crews CM, Clardy J. Structure of human methionine aminopeptidase-2 complexed with fumagillin. Science. 1998; 282: 1324-7.
26. Zhou H-f, Yan H, Senpan A, Wickline SA, Pan D, Lanza GM, et al. Suppression of inflammation in a mouse model of rheumatoid arthritis using targeted lipase-labile fumagillin prodrug nanoparticles. Biomaterials. 2012; 33: 8632-40.
27. Hu S, Wang LV. Photoacoustic imaging and characterization of the microvasculature. J Biomed Opt. 2010; 15: 011101.
28. Meng-Lin L, Jung-Taek O, Xie X, Ku G, Wei W, Chun L, et al. Simultaneous Molecular and Hypoxia Imaging of Brain Tumors In Vivo Using Spectroscopic Photoacoustic Tomography. Proceedings of the IEEE. 2008; 96: 481-9.
29. Rouleau L, Berti R, Ng VW, Matteau-Pelletier C, Lam T, Saboural P, et al. VCAM-1-targeting gold nanoshell probe for photoacoustic imaging of atherosclerotic plaque in mice. Contrast Media Mol Imaging. 2013; 8: 27-39.
30. Kim C, Cho EC, Chen J, Song KH, Au L, Favazza C, et al. In vivo molecular photoacoustic tomography of melanomas targeted by bioconjugated gold nanocages. ACS nano. 2010; 4: 4559-64.
31. Li P-C, Wang C-RC, Shieh D-B, Wei C-W, Liao C-K, Poe C, et al. In vivo photoacoustic molecular imaging with simultaneous multiple selective targeting using antibody-conjugated gold nanorods. Opt Express. 2008; 16: 18605-15.
32. Agarwal A, Huang S, O'Donnell M, Day K, Day M, Kotov N, et al. Targeted gold nanorod contrast agent for prostate cancer detection by photoacoustic imaging. J Appl Phys. 2007; 102: 064701.
33. Zerda Adl, Liu Z, Bodapati S, Teed R, Vaithilingam S, Khuri-Yakub BT, et al. Ultrahigh sensitivity carbon nanotube agents for photoacoustic molecular imaging in living mice. Nano letters. 2010; 10: 2168-72.
34. Pan D, Caruthers SD, Senpan A, Yalaz C, Stacy AJ, Hu G, et al. Synthesis of NanoQ, a copper-based contrast agent for high-resolution magnetic resonance imaging characterization of human thrombus. J Am Chem Soc. 2011; 133: 9168-71.
35. Schmieder AH, Winter PM, Caruthers SD, Harris TD, Williams TA, Allen JS, et al. Molecular MR imaging of melanoma angiogenesis with alphanubeta3-targeted paramagnetic nanoparticles. Magn Reson Med. 2005; 53: 621-7.
36. Winter PM, Caruthers SD, Kassner A, Harris TD, Chinen LK, Allen JS, et al. Molecular imaging of angiogenesis in nascent Vx-2 rabbit tumors using a novel alpha(nu)beta3-targeted nanoparticle and 1.5 tesla magnetic resonance imaging. Cancer Res. 2003; 63: 5838-43.
37. Jain RK. Normalizing tumor vasculature with anti-angiogenic therapy: a new paradigm for combination therapy. Nat Med. 2001; 7: 987-9.
38. Jain RK. Taming vessels to treat cancer. Sci Am. 2008; 298: 56-63.
39. Jain RK, Finn AV, Kolodgie FD, Gold HK, Virmani R. Antiangiogenic therapy for normalization of atherosclerotic plaque vasculature: a potential strategy for plaque stabilization. Nat Clin Pract Cardiovasc Med. 2007; 4: 491-502.
40. Lee J, Ku T, Yu H, Chong K, Ryu SW, Choi K, et al. Blockade of VEGF-A suppresses tumor growth via inhibition of autocrine signaling through FAK and AKT. Cancer Lett. 2012; 318: 221-5.
41. Eskens FA, Verweij J. The clinical toxicity profile of vascular endothelial growth factor (VEGF) and vascular endothelial growth factor receptor (VEGFR) targeting angiogenesis inhibitors; a review. Eur J Cancer. 2006; 42: 3127-39.
42. Offodile R, Walton T, Lee M, Stiles A, Nguyen M. Regression of metastatic breast cancer in a patient treated with the anti-angiogenic drug TNP-470. Tumori. 1999; 85: 51-
43. Herbst RS, Madden TL, Tran HT, Blumenschein GR, Jr., Meyers CA, Seabrooke LF, et al. Safety and pharmacokinetic effects of TNP-470, an angiogenesis inhibitor, combined with paclitaxel in patients with solid tumors: evidence for activity in non-small-cell lung cancer. J Clin Oncol. 2002; 20: 4440-7.
44. Logothetis CJ, Wu KK, Finn LD, Daliani D, Figg W, Ghaddar H, et al. Phase I trial of the angiogenesis inhibitor TNP-470 for progressive androgen-independent prostate cancer. Clin Cancer Res. 2001; 7: 1198-203.
45. Winter PM, Caruthers SD, Zhang H, Williams TA, Wickline SA, Lanza GM. Antiangiogenic synergism of integrin-targeted fumagillin nanoparticles and atorvastatin in atherosclerosis. JACC Cardiovasc Imaging. 2008; 1: 624-34.
46. Winter PM, Schmieder AH, Caruthers SD, Keene JL, Zhang H, Wickline SA, et al. Minute dosages of alpha(nu)beta3-targeted fumagillin nanoparticles impair Vx-2 tumor angiogenesis and development in rabbits. FASEB J. 2008; 22: 2758-67.
47. Soman NR, Baldwin SL, Hu G, Marsh JN, Lanza GM, Heuser JE, et al. Molecularly targeted nanocarriers deliver the cytolytic peptide melittin specifically to tumor cells in mice, reducing tumor growth. J Clin Invest. 2009; 119: 2830-42.
48. Partlow KC, Lanza GM, Wickline SA. Exploiting lipid raft transport with membrane targeted nanoparticles: a strategy for cytosolic drug delivery. Biomaterials. 2008; 29: 3367-75.
49. Pan D, Schmieder AH, Wang K, Yang X, Senpan A, Cui G, et al. Anti-angiogenesis therapy in the Vx2 rabbit cancer model with a lipase-cleavable sn 2 taxane phospholipid prodrug using alphavbeta3-targeted theranostic nanoparticles. Theranostics. 2014; 4: 565-78.
50. Zhou HF, Yan H, Hu Y, Springer LE, Yang X, Wickline SA, et al. Fumagillin Prodrug Nanotherapy Suppresses Macrophage Inflammatory Response via Endothelial Nitric Oxide. ACS Nano. 2014; 8: 7305-17.